An Embroidered Slot-Loaded Patch Antenna for Characterization of Dielectric Materials

Michael Elsdon[1, *], Shahrzad Zahertar[2], Hamdi Torun[1], and Linzi E. Dodd[1]

Abstract—Embroidery has been recently introduced as a new method to realize sensors especially for wearables. In this paper, we present a slot-loaded embroidered patch antenna to provide a simplified setup which allows the antenna to act as a stand-alone resonator. The design procedure, simulation, and implementation of an embroidered sensor are presented and discussed. It is demonstrated that this structure can be used without any need for external antennas as a wireless sensor. To demonstrate the feasibility of this technique, the design process using a slot-loaded antenna to achieve a high Q antenna, fabricated on an FR4 substrate, is presented and discussed. This structure is then manufactured, with practical results shown to agree with simulated results. Using this as a basis for subsequent designs, an embroidered slot-loaded patch is presented and discussed. We demonstrate this capability in an experiment where a set of solvents inside plastic bottles were interrogated using the embroidered antennas.

1. INTRODUCTION

Embroidery has been recently introduced as a new method to realize sensors especially for wearables. Different configurations have been introduced for several applications. Conductive yarns can be used as interconnects to attach electronic chips and components on textile-based substrates [1]. Use of conductive yarns as electrodes was also demonstrated to obtain ECG signals [2] and bio impedance measurements [3]. In addition, textiles with functional electrical properties have been demonstrated. For example, resistive textiles for pressure sensing [4] and strain sensing [5] have been introduced for biomedical monitoring. Functionalization of the threads embroidered into fabric has been proposed to develop electrochemical sensors for wound monitoring [6] and continuous biomarker monitoring [7] applications. The capability of embroidering highly conductive threads into dielectric fabric-based substrates allows developing antennas for different applications. For example, Xu et al. proposed antenna structures for near field communications [8]. Also, ultra-wide band antennas have been demonstrated [9, 10]. Conformity is an obvious advantage in these configurations [11], and the optimization of parameters has been investigated for these applications [12]. In addition to wide band antennas for communication applications, resonant structures can be realized using embroidery as sensors. In this approach, the resonant frequency of the structure is a function of its geometry and the electrical parameters of its surroundings. So, the resonant frequency of the structure can be tracked as a sensing mechanism. Split-ring resonator-based embroidered structure is an example for this method and has been previously employed to characterize various dielectric solvents when the substrate is conformally wrapped around samples [13]. This implementation requires a pair of monopole antennas coupled to the resonator for measurements.

In this paper, we present a slot-loaded embroidered patch antenna to provide a simplified setup to allow the antenna itself to act as a stand-alone resonator. We explain the design methodology and present the validation results for the design using a test structure fabricated on a well characterized FR4 substrate following a conventional PCB fabrication technique. Accordingly, in Section 2, we demonstrate the design process for a slot-loaded antenna to be optimized for sensing applications, with the initial design fabricated on an FR4 PCB. Section 3 presents the simulation and experimental characterization of the proposed design. Using this as a basis for future design, in Section 4, an embroidered patch antenna is used to characterize various solvents without the need for excitation using external antennas for the measurements.

2. ANTENNA DESIGN METHODOLOGY

This section outlines the design process for developing reduced size antennas for sensing applications. For sensing applications, it is beneficial to have a small antenna with high Q and optimum impedance matching to achieve maximum power transfer. In recent years considerable progress has been made in the design of compact patch antennas. The use of slot loading is a well-known technique for reducing the size of the patch antenna and has been the subject of many studies. In such designs, the insertion of slots results in the perturbation of different TM_{mn} modes. The modes which are affected and to what extent are dependent on the slot shape and dimensions, together with its position. By correct perturbation of the TM_{01} mode, it is possible to reduce the size of the patch antenna. Common techniques for exciting the patch include probe, aperture-couple, proximity couple, or planar feed. The use of a planar feed has inherent advantages over other techniques as it not only eliminates drilling of holes and probe soldering, but also makes it easy to impedance match via the use of quarter-wave matching or the use of an inset feed. Moreover, the use of a planar feed allows easier manufacturing, robustness, and ease of integration with associated microwave circuitry. In particular, this is advantageous for applications requiring conformity such as wearables. A typical reduced size patch antenna with square slot loading is shown in Figure 1.
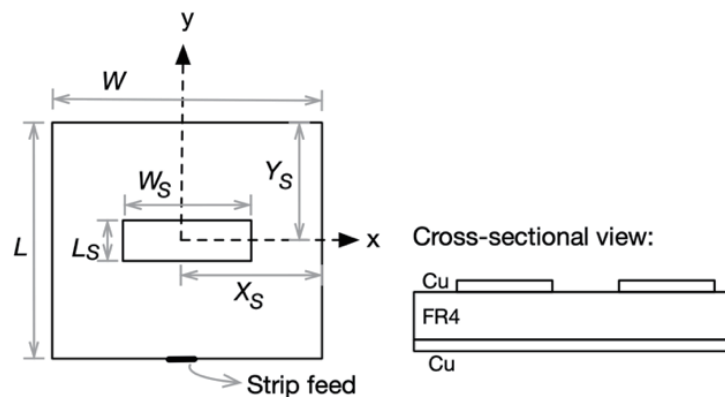
**Figure 1.** Slot loaded patch antenna design.

The patch antenna was fabricated on an FR4 PCB with a permittivity of 4.5 and thickness 1.57 mm. The patch dimensions L and W were both fixed at 48 mm to produce an unmodified resonant frequency of 3.17 GHz. These dimensions were chosen to keep the overall patch dimensions smaller to reduce manufacturing costs. The patch was excited using a 50 Ω microstrip feed at the patch edge ($x = 0$, $y = W/2$) to excite the TM_{01} mode. The individual slot parameters are related to slot length (L_s), slot width (W_s), slot position with respect to x direction (x_s), and slot position with respect to y direction (y_s). To this end, all results refer to the effect on TM_{01} mode. Parametric analysis of this design has been performed to determine the effect of different slot parameters on antenna circuit characteristics. This knowledge has been used as a basis for the design of a high Q antenna for sensing applications.
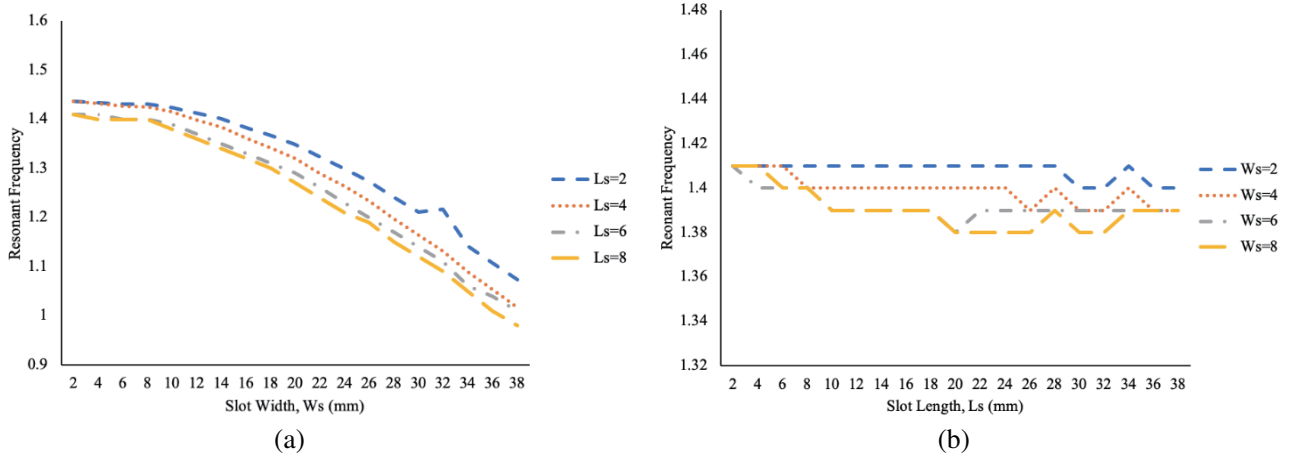
Figure 2. Effect of (a) slot width and (b) slot length on resonant frequency, where $L = W = 48\,\text{mm}$, $x_s = y_s = 15\,\text{mm}$, $\varepsilon r = 4.5$, $h = 1.57\,\text{mm}$.

The results in Figures 2(a), (b) demonstrate the relationship between slot parameters and patch antenna resonant frequency. Regarding the effect of slot width, it is observed that for all values of slot length, there is a significant reduction in antenna resonant frequency with increased slot width. When $Ls = 8\,\text{mm}$, the resonant frequency is reduced from $1.41\,\text{GHz}$ to $0.98\,\text{GHz}$ over a slot width of $0\,\text{mm}$ to $38\,\text{mm}$. Regarding the effect of slot length, with a narrow slot width ($Ws = 2\,\text{mm}$), it is observed that increasing slot length has negligible effect on the antenna resonant frequency, producing a frequency reduction from $1.41\,\text{GHz}$ to $1.4\,\text{GHz}$. It is also observed that for increased values of slot width, the value of slot length affects the resonant frequency. For the case of a large slot width ($Ws = 8\,\text{mm}$), the resonant frequency is reduced from $1.41\,\text{GHz}$ to $1.39\,\text{GHz}$, representing a frequency reduction of $0.01\,\text{GHz}$. From the above results it can be concluded that slot width has the greatest effect on the resonant frequency of the TM_{01} mode, whilst the slot length has negligible effect.

The results in Figures 3(a), (b) demonstrate the relationship between slot parameters and patch antenna Q factor. As with resonant frequency, slot width is the major controlling slot parameter governing Q factor and hence bandwidth. This trend is evidenced in Figure 3, which illustrates that for all values of slot length, there is a significant increase in antenna Q factor with increasing slot width. Increasing Q factor is advantageous for sensing applications where the resonant frequency of the antenna is tracked. The resonant frequency of the structure is determined by the geometry of the
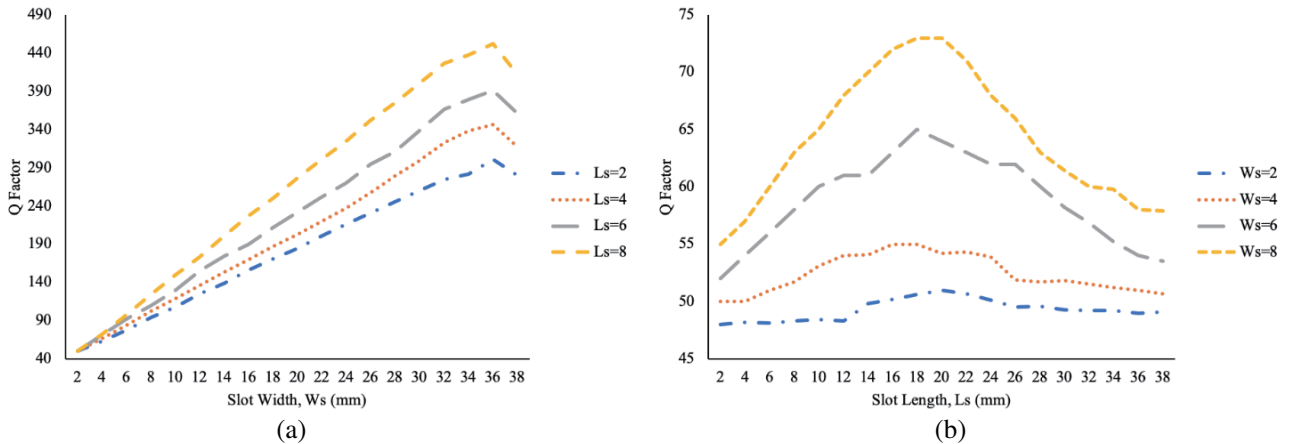
Figure 3. Effect of (a) slot width and (b) slot length on Q factor, where $L = W = 48\,\text{mm}$, $x_s = y_s = 15\,\text{mm}$, $\varepsilon r = 4.5$, $h = 1.57\,\text{mm}$.

structure together with the effective electric permittivity and magnetic permeability of the environment that the structure is placed in. This has been used as a sensing mechanism for strain sensors with structures that undergo geometrical changes [14, 15]. If the geometry of the structure does not change, then the changes in the environment can be sensed if they alter the effective electrical permittivity or magnetic permeability of the structures. Several applications including measurement of biomolecular interactions [16, 17], concentration of target solutions [18, 19], and material characterization [13, 20] have been demonstrated so far. The resolution of the measurement based on tracking the resonant frequency is determined by the quality factor for these applications.

The results in Figures 4(a), (b) demonstrate the relationship between slot parameters and patch antenna input impedance. It can be seen that whilst increasing slot length provides benefits in terms of size reduction and increased Q factor, it produces an increased patch antenna input impedance. This creates a challenge with respect to impedance matching. By examining Figure 4, for a fixed value of slot width, for example $Ws = 38$ mm, if slot length Ls is further increased, it creates two problems. Firstly, the value of input impedance increases further, making it difficult to impedance match. Moreover, increasing slot length reduces the physical space for an inset feed. So, it is a design challenge to reduce frequency and increase Q factor, whilst simultaneously maintaining an input impedance of practical value to allow impedance matching.
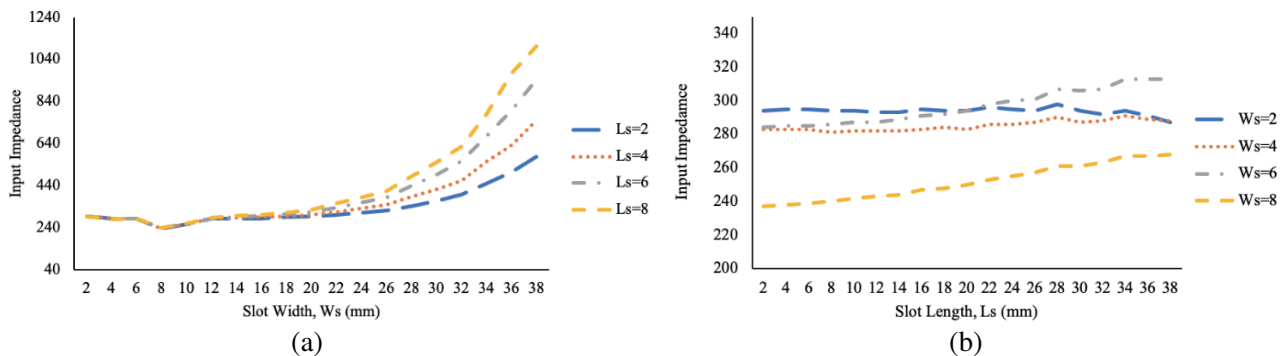
Figure 4. Effect of (a) slot width and (b) slot length on input impedance, where $L = W = 48$ mm, $x_s = y_s = 15$ mm, $\varepsilon r = 4.5$, $h = 1.57$ mm.

Regarding the slot position, the slot has maximum effect on the TM_{01} mode when it is positioned along the central x axis of the patch, with its effect decreasing as it moves towards the patch edge. The same relationship can also be expected to exist between y position and the characteristics of the TM_{10} mode.

The presented design is scalable and can be adapted for different frequency bands. The operation frequency can be selected by scaling the geometry presented here. Our selection is based on a geometry that can be manufactured easily using methods of embroidery while obtaining high Q factors for sensing applications.

3. PCB DESIGN

3.1. Design

For sensing applications, the goal is to achieve maximizing antenna Q factor, whilst maintaining an input impedance of practical value to allow impedance matching, with a reduction in antenna size also being beneficial. From the investigation performed in the previous section, significant trade-offs exist among all these performance characteristics, and it is not possible to simultaneously optimize each one.

Using the knowledge obtained from this study, a slot loaded patch antenna based on the structure illustrated in Figure 5 has been designed. The design presented in this section allows the use of a direct planar feed with increased Q factor, thus removing the requirement for an external impedance matching
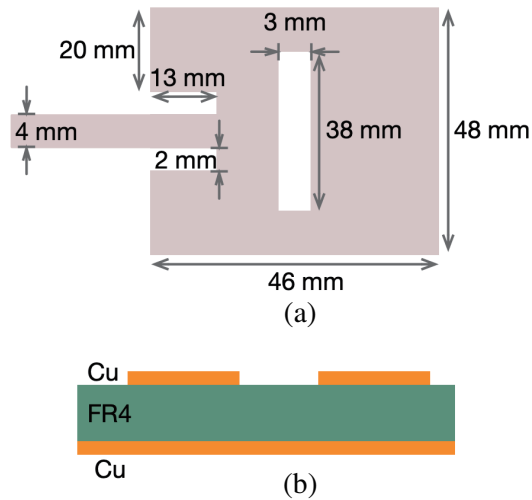
Figure 5. (a) Proposed patch structure and its geometry as implemented on (b) an FR4 substrate with two Cu layers used as a ground plane and to define the structure.

network and hence further reducing overall antenna size. A prototype of the design, shown in Figure 1, was fabricated on an FR4-PCB, with relative permittivity 4.5 and thickness 1.57 mm. The proposed design has patch length, L, and width, W, of 48 mm, with a slot of length l_1 of 46 mm and w_1 of 3 mm and is located at the center of the patch. To achieve impedance matching, an inset feed was used with a value of slit length, $1_f = 13$ mm, which was determined using parametric analysis. The value of slit width was arbitrary and set to $W_f = 2$ mm.

3.2. Simulation

We performed simulations for the patch antenna on an FR4 substrate within the frequency range of 0.5–3.5 GHz in CST Microwave Studio, and results are shown in Figure 6. Figure 6(a) represents the S_{11} parameters of the slot patch antenna, and multiple sharp frequencies can be observed within the intended range. The first fundamental frequency happens at 0.97 GHz, and the second frequency with the highest quality factor happens at 3.12 GHz. The electric field (E-field) and current density patterns for these frequencies are shown in Figures 6(c)–(e), respectively. Observation of the current density pattern can help identify the behavior of the resonator and indicate the most sensitive parts of the sensor.

As can be seen from Figure 6(c) for the frequency of 0.97 GHz, the density of the current is more prominent on the edges of the slot in the patch antenna compared to other regions, and therefore, altering the medium around these edges can have a more profound impact in the resonant frequency. This frequency is used as a sensing element later in the experiments. Figure 6(e) represents the distribution of the current at the frequency of 3.12 GHz. In this frequency, the current is distributed on the half side of the antenna, which is connected to the excitation port, and no current is generated on the other half.

3.3. Experimental Characterization

We characterized the fabricated patch antenna on an FR4 substrate by connecting it to a port of a Vector Network Analyzer (VNA, Agilent Technologies, N5230A) through an SMA connector. We measured the reflection coefficient (S_{11}) of the antennas. The characterization setup and the captured S_{11} result are shown in Figure 7.

The sharp frequencies can be observed at 1.07 and 2.94 GHz, respectively, which are in a good agreement with the data presented in Figure 6(a). The slight discrepancies could be attributed to the differences in dielectric constant tolerances, manufacturing errors, and the equations used are non-closed form. We also observed a directivity of 6 dBi and a radiation efficiency of -21 dB at 1.07 GHz.

(a)

(b)

(c)

(d)

(e)
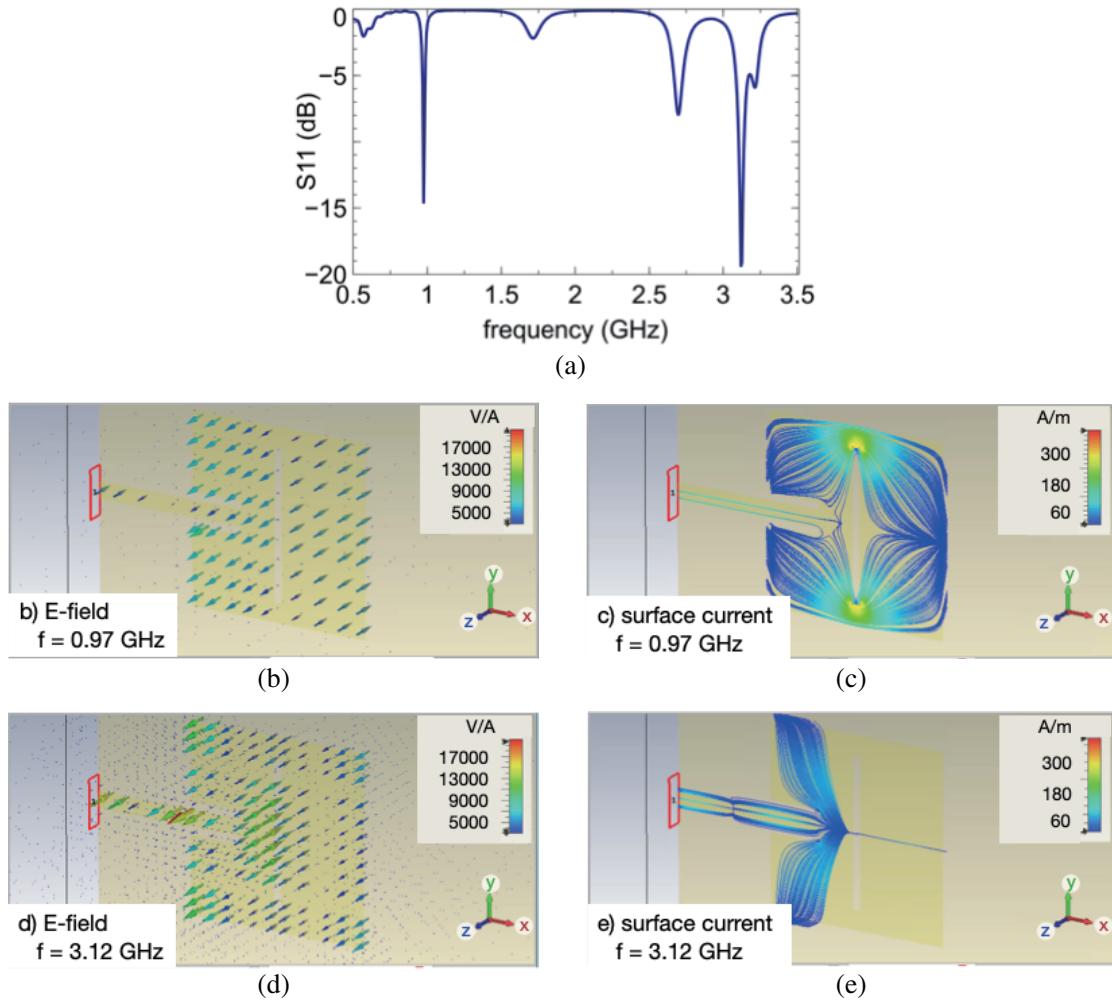
Figure 6. (a) S_{11} characteristics of the design with the frequency range of 0.5–3.5 GHz. (b) Electric field distribution at the frequency of 0.97 GHz. (c) Current density pattern of the patch antenna at 0.97 GHz. (d) Electric field distribution at the frequency of 3.12 GHz. (e) Current density pattern of the patch antenna at 3.12 GHz.
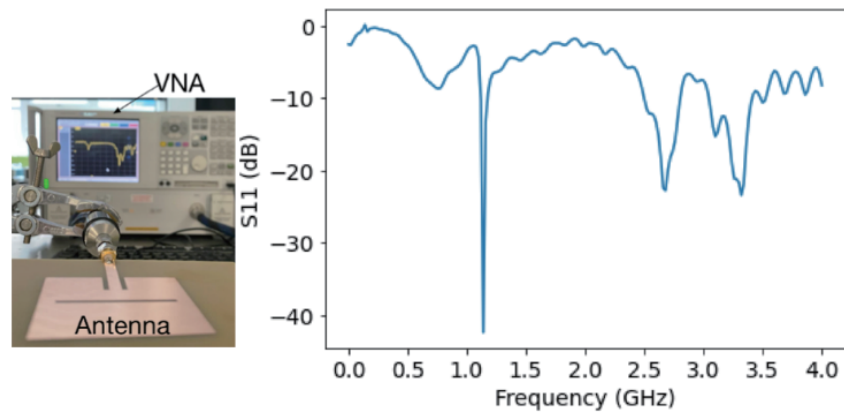

Figure 7. Setup and the S_{11} spectrum of the slot patch antenna on an FR4 substrate.

4. EMBROIDERED DESIGN

4.1. Fabrication

After we validated our slot-loaded patch antenna design using PCB manufacturing techniques, we investigated methods to realize this design using embroidery with conductive threads. Based upon the results from the previous section, we fabricated an embroidered antenna with dimensions as shown in Figure 8(a), (Brother PR1050X) with conductive threads on a 0.25 mm thick calico textile substrate. The stack-up of the structure can be seen in Figure 8(b). Different conductive threads were tested, including Syscom Advanced Materials Amberstrand 166 [21] and Liberator 40 [22] threads, both of which are silver-coated threads with 166 and 40 fibers strands, respectively. Both threads are highly conductive, with a resistance of 1 Ohm/ft.
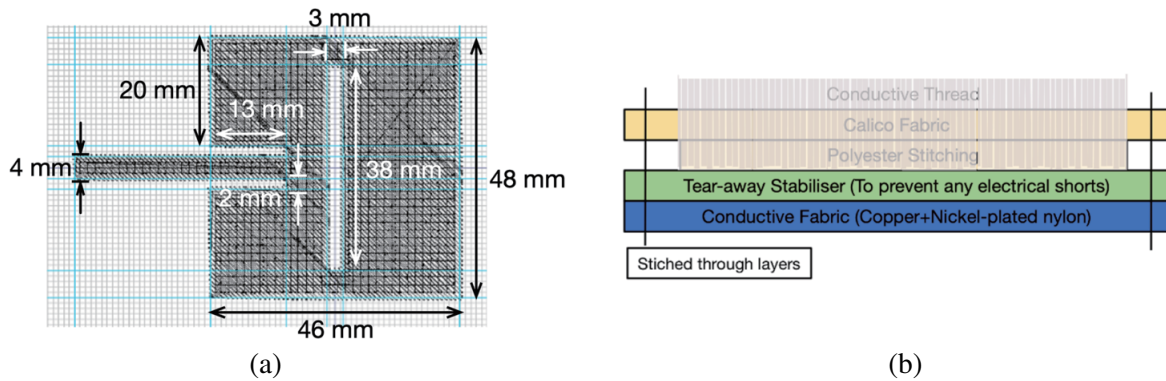

Figure 8. (a) design and dimensions of the slot-loaded patch antenna in PE Design and (b) a cross-sectional diagram of the embroidered stack, showing the calico fabric with the embroidered antenna, a layer of tearaway fabric to prevent any electrical shorting caused by any stray thread fibres, and the base conductive thread layer.

The antenna pattern was designed with a dense under-sew with 3.4 lines/mm. The under-sew pattern runs both horizontally and vertically to create a grid of small square shapes, with the antenna pattern on top, running at a 45-degree angle, which provides a good electrical connection throughout. To improve the accuracy of the final device measurements, a 0.5 mm pull compensation was included. This ensures that any compression caused by the high-density stitches does not affect the final dimensions of the antenna. This amount of compensation was determined iteratively. The central slot was also stitched with a larger slot length, Ls, than originally specified, i.e., 3 mm rather than 2 mm, as the size of the gap is reduced by the nature of the fabrication process. As demonstrated in Figure 2(b), the effect of the slot length on the resonant frequency of the design is minimal, so this will have little effect on the results. The final device was completed by combining the antenna layer with a tearaway stabilizer layer to prevent any electrical shorts and a conductive fabric layer, consisting of copper (16%) and nickel (14%)-plated nylon [23] which is 0.08 ± 0.01 mm thick and acts as the ground plane.

4.2. Simulation

A CST model of Figure 8 was created, with a gridded structure to simulate both the ground and patch layer, whilst calico material was used for the substrate. The simulated return loss of this structure is shown in Figure 9(a), which demonstrates a return loss of -19 dB at 1.84 GHz. The far field directivity at 1.84 GHz is shown in Figures 9(b) and 9(c), for Phi = 0° and Phi = 90°, respectively. Figure 9(b) demonstrates a directivity of 7.42 dBi, with a main lobe direction of 2 degrees and a 3 dB beamwidth of 78.8°. Figure 9(c) demonstrates a directivity of 7.42 dBi, with a main lobe direction of 0 degrees and a 3 dB beamwidth of 89.1°.
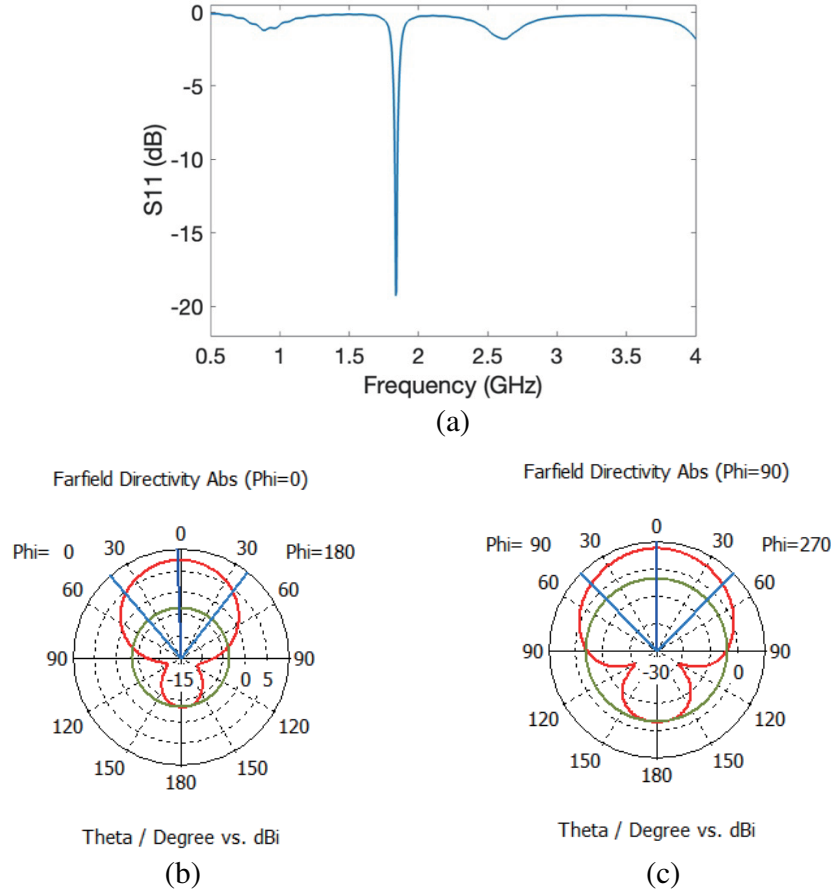
Figure 9. S_{11} characteristics of the design with the frequency range of 0.5–2.5 GHz, (b) Far-field pattern at the frequency of 1.84 GHz (phi = 0), (c) Far-field pattern at 1.84 GHz (phi = 90).

4.3. Sensing Experimental Results and Discussion

In the next step, we characterized the embroidered slot patch antenna with the same method. Fabricated patch antennas were interrogated using the VNA and by measuring the spectra of their reflection coefficients (S_{11}). For comparison purposes, we plotted the experimental characterization of the slot patch antenna on an FR4 substrate and the embroidered slot patch antenna in Figures 10(a) and (b), respectively. The fundamental resonant frequency of the antenna on the FR4 substrate, as discussed previously, is 1.07 GHz, while the fundamental resonant frequency of the embroidered antenna is 1.97 GHz. This can be explained by the different materials used for the fabrication and the exact dimension of the fabricated structures. The relative permittivity of the FR4 is 4.4, whereas the relative permittivity of the cloth is ~ 1.6 [24]. This difference will change the effective capacitance of the resonator and therefore lead to a change in the fundamental resonant frequency. In addition, maintaining the exact features and dimensions of the resonator can be more challenging when the device is fabricated through an embroidery machine versus a standard printed circuit board (PCB) technique. We also observed a directivity of 6 dBi and a radiation efficiency of -15.24 dB at 1.97 GHz.

For sensing experiments, we used the embroidered antenna to measure the characteristics of low-density polyethylene (LDPE) bottles filled with various solvents including methanol, ethanol, acetone, and IPA. The frequency response of the embroidered antenna is shown in Figure 10(a). We used an empty bottle as a reference during the measurements. Then bottles were placed sequentially in front of the patch antennas closer to the edge of the slit, and S_{11} spectra were captured for each experiment. The sequence was repeated for five times to ensure the repeatability of the measurements. Figure 10(b) illustrates the representative data for each of the solvent. Figure 10(c) shows the average frequency

(a)

(b)

(c)
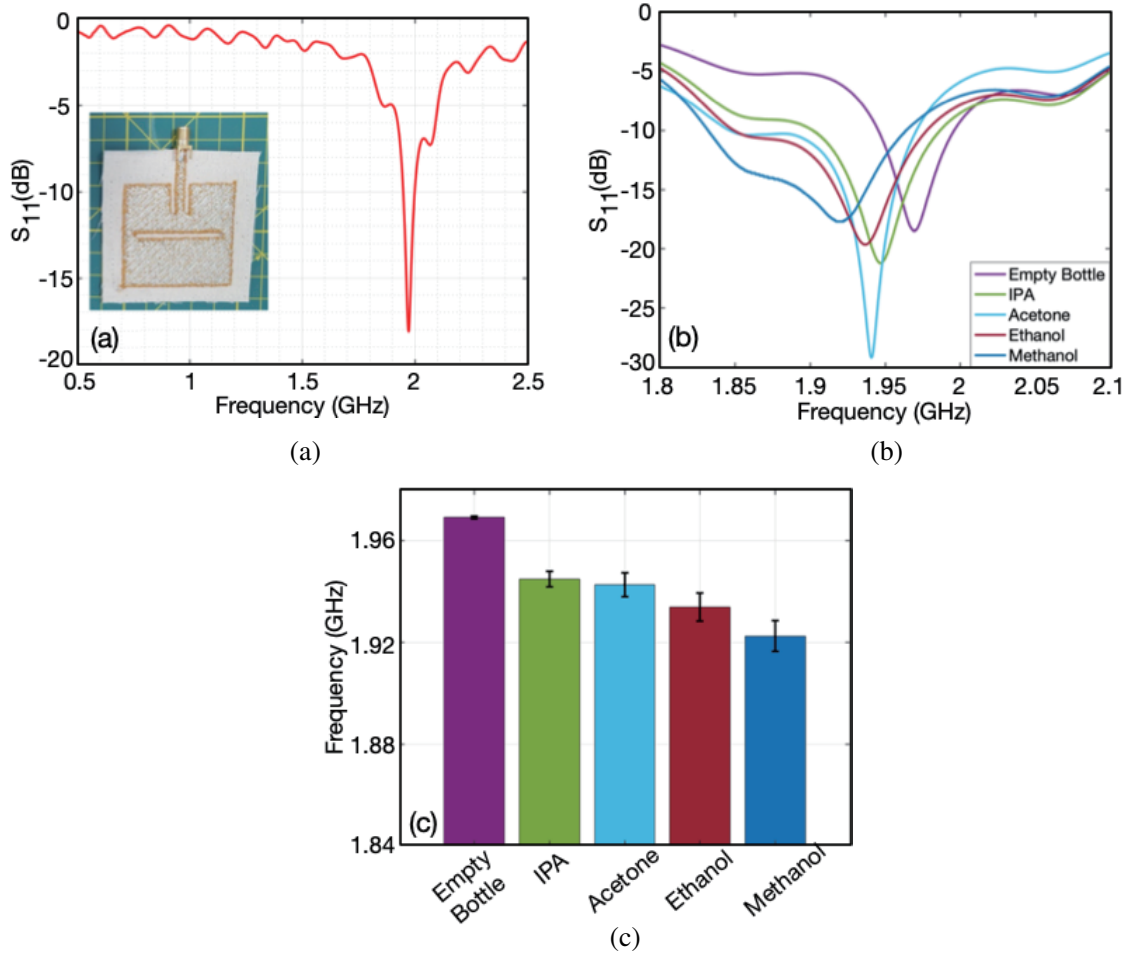
Figure 10. (a) Experimental characterization of the embroidered slot patch antenna fabricated on fabric. (b) Representative S_{11} spectra of solvents when the bottle was placed in front of the embroidered patch antenna. (c) The average resonant frequency and the standard deviation obtained for each solvent.

obtained in the experiments for each solvent, and the error bars represent the standard deviation. The results are also summarized in Table 1.

The relative permittivity of the methanol, ethanol, acetone, IPA, and air is 32.6, 24.3, 20.6, 18.3, and 1, respectively [25]. As discussed earlier, a change in effective permittivity of the medium surrounding the resonator will change the effective capacitance of the resonator, and therefore, a shift in the resonant frequency is expected. Higher permittivity value in the solvents increases the effective capacitance and

Table 1. Material Properties and mean value of measured frequencies for solvents.

	Relative Permittivity	Resonant Frequency (Mean ± Standard Deviation) (GHz)
Methanol	32.6	1.92 ± 0.0060
Ethanol	24.3	1.93 ± 0.0056
Acetone	20.6	1.94 ± 0.0047
Isopropanol Alcohol	18.3	1.95 ± 0.0031
Air (Empty Bottle)	1	1.97 ± 0.0006

decreases the resonant frequency. The obtained results, which are summarized in Table 1 and plotted in Figures 9(c)–(d), are in agreement with our expectations; the highest resonant frequency corresponds to the case where bottle is empty (lowest relative permittivity), and the lowest resonant frequency corresponds to the experiment, where the bottle is filled with methanol (highest relative permittivity).

5. CONCLUSION

In this paper, a method of realizing antenna-based sensors using embroidery with conductive threads was presented. For the demonstration, we designed a slot-loaded patch antenna and validated the design using a fabricated structure with conventional PCB manufacturing techniques on an FR4 substrate. The resonant frequency of the simulated structure is at 0.97 GHz, and the measured resonant frequency for the structure realized on the FR4 substrate is at 1.14 GHz. The simulated and measured quality factors exceed 50. Our simulations agree with the measurement results, validating the slot-loaded patch antenna design. We discuss the effect of geometric parameters on the electromagnetic behavior of the design. Then, we implemented the design on a fabric using conductive threads. The fabricated structure maintains a distinct resonant frequency at 1.97 GHz with a high-quality factor suitable for sensing applications. Thus, as opposed to resonators that require coupling with external antennas, this structure can be used alone as a wireless sensor. We demonstrated this capability in an experiment where a set of solvents inside plastics bottles were interrogated using the embroidered antennas. We measured a shift of 50 MHz in resonant frequencies when the embroidered antenna was loaded with methanol with a relative permittivity of 32.6.

REFERENCES

1. Linz, T., C. Kallmayer, R. Aschenbrenner, and H. Reichl, "Embroidering electrical interconnects with conductive yarn for the integration of flexible electronic modules into fabric," *Proc. — Int. Symp. Wearable Comput. ISWC*, Vol. 2005, 86–89, 2005, doi: 10.1109/ISWC.2005.19.

2. Weder, M., D. Hegemann, M. Amberg, et al., "Embroidered electrode with silver/titanium coating for long-term ECG monitoring," *Sensors 2015*, Vol. 15, Vol. 15, No. 1, 1750–1759, Jan. 2015, doi: 10.3390/S150101750.

3. Logothetis, I., D. Vatansever Bayramol, I. Gil, Dabnichki, and E. Pirogova, "Evaluating silver-plated nylon (Ag/PA66) e-textiles for bioelectrical impedance analysis (BIA) application," *Meas. Sci. Technol.*, Vol. 31, No. 7, Jul. 2020, doi: 10.1088/1361-6501/AB78C3.

4. Aigner, R., A. Pointner, T. Preindl, Parzer, and M. Haller, "Embroidered resistive pressure sensors: A novel approach for textile interfaces," *Conf. Hum. Factors Comput. Syst. — Proc.*, Apr. 2020, doi: 10.1145/3313831.3376305.

5. Atalay, O., W. R. Kennon, and E. Demirok, "Weft-knitted strain sensor for monitoring respiratory rate and its electro-mechanical modelling," *IEEE Sens. J.*, Vol. 15, No. 1, 110–122, Jan. 2015, doi: 10.1109/JSEN.2014.2339739.

6. Liu, X. and B. Lillehoj, "Embroidered electrochemical sensors for biomolecular detection," *Lab Chip*, Vol. 16, No. 11, 2093–2098, May 2016, doi: 10.1039/C6LC00307A.

7. Liu, X. and B. Lillehoj, "Embroidered electrochemical sensors on gauze for rapid quantification of wound biomarkers," *Biosens. Bioelectron.*, Vol. 98, 189–194, Dec. 2017, doi: 10.1016/J.BIOS.2017.06.053.

8. Xu, L., Z. Liu, X. Chen, et al., "Deformation-resilient embroidered near field communication antenna and energy harvesters for wearable applications," *Adv. Intell. Syst.*, Vol. 1, No. 6, 1900056, Oct. 2019, doi: 10.1002/AISY.201900056.

9. Sim, C. Y. D., C. W. Tseng, and H. J. Leu, "Embroidered wearable antenna for ultrawideband applications," *Microw. Opt. Technol. Lett.*, Vol. 54, No. 11, 2597–2600, Nov. 2012, doi: 10.1002/MOP.27133.

10. Manohar, M., R. S. Kshetrimayum, and A. K. Gogoi, "A compact printed triangular monopole antenna for ultrawideband applications," *Microw. Opt. Technol. Lett.*, Vol. 56, No. 5, 1155–1159, May 2014, doi: 10.1002/MOP.28290.

11. Wang, Z., L. Zhang, Y. Bayram, and J. L. Volakis, "Embroidered conductive fibers on polymer composite for conformal antennas," *IEEE Trans. Antennas Propag.*, Vol. 60, No. 9, 4141–4147, 2012, doi: 10.1109/TAP.2012.2207055.

12. Ivsic, B., D. Bonefacic, and J. Bartolic, "Considerations on embroidered textile antennas for wearable applications," *IEEE Antennas Wirel. Propag. Lett.*, Vol. 12, 1708–1711, 2013, doi: 10.1109/LAWP.2013.2297698.

13. Zahertar, S., E. Laurin, L. E. Dodd, and H. Torun, "Embroidered rectangular split-ring resonators for the characterization of dielectric materials," *IEEE Sens. J.*, 1–1, 2019, doi: 10.1109/JSEN.2019.2953251.

14. Melik, R., E. Unal, N. K. Perkgoz, C. Puttlitz, and H. V. Demir, "Metamaterial-based wireless strain sensors," *Appl. Phys. Lett.*, Vol. 95, No. 1, 011106, Jul. 2009, doi: 10.1063/1.3162336.

15. Ekinci, G., A. Calikoglu, S. N. Solak, A. D. Yalcinkaya, G. Dundar, and H. Torun, "Split-ring resonator-based sensors on flexible substrates for glaucoma monitoring," *Sensors Actuators A Phys.*, Vol. 268, 32–37, Dec. 2017, doi: 10.1016/J.SNA.2017.10.054.

16. Torun, H., F. C. Top, G. Dundar, and A. D. Yalcinkaya, "An antenna-coupled split-ring resonator for biosensing," *J. Appl. Phys.*, Vol. 116, No. 12, 124701, Sep. 2014, doi: 10.1063/1.4896261.

17. Lee, H.-J., H.-S. Lee, K.-H. Yoo, and J.-G. Yook, "DNA sensing using split-ring resonator alone at microwave regime," *J. Appl. Phys.*, Vol. 108, No. 1, 014908, Jul. 2010, doi: 10.1063/1.3459877.

18. Camli, B., E. Altinagac, H. Kizil, H. Torun, G. Dundar, and A. D. Yalcinkaya, "Gold-on-glass microwave split-ring resonators with PDMS microchannels for differential measurement in microfluidic sensing," *Biomicrofluidics*, Vol. 14, No. 5, 054102, Sep. 2020, doi: 10.1063/5.0022767.

19. Govind, G. and M. J. Akhtar, "Metamaterial-inspired microwave microfluidic sensor for glucose monitoring in aqueous solutions," *IEEE Sens. J.*, Vol. 19, No. 24, 11900–11907, Dec. 2019, doi: 10.1109/JSEN.2019.2938853.

20. Ebrahimi, A., W. Withayachumnankul, S. Al-Sarawi, and D. Abbott, "High-sensitivity metamaterial-inspired sensor for microfluidic dielectric characterization," *IEEE Sens. J.*, Vol. 14, No. 5, 1345–1351, 2014, doi: 10.1109/JSEN.2013.2295312.

21. Syscom Advanced Materials, "Amberstrand 166," metalcladfibers.com, 2018. https://static1.squarespace.com/static/558431b9e4b0875de16c5494/t/5d9d011bb7bacf1e9e34d93c-/1570570527783/Amberstrand+166.pdf (accessed Oct. 28, 2021).

22. Syscom Advanced Materials, "Liberator 40," metalcladfibers.com, 2018. https://static1.squarespace.com/static/558431b9e4b0875de16c5494/t/5d9d012db7bacf1e9e34dc86-/1570570546216/Liberator+40.pdf (accessed Oct. 28, 2021).

23. Adafruit, "Adafruit Conductive Fabric Datasheet," adafruit.com. https://cdn-shop.adafruit.com/product-files/1168/Pn1168_Datasheet.pdf (accessed Oct. 28, 2021).

24. Ibanez-Labiano, I. and A. Alomainy, "Dielectric Characterization of Non-Conductive Fabrics for Temperature Sensing through Resonating Antenna Structures," *Mater. 2020*, Vol. 13, No. 6, 1271, Mar. 2020, doi: 10.3390/MA13061271.

25. Smallwood, I. M., *Handbook of Organic Solvent Properties*, Elsevier Ltd., 1996.